Asociación Argentina
de Mecánica Computacional

Mecánica Computacional Vol XLII, pp. 453-462
A. Caggiano, G. Etse, P. Folino, M. Goldschmit, M. Pucheta, M. Storti (Eds.)
L. Battaglia, H. Castro, M. Coussirat, R. Paz, S. Sarraf, A. Scarabino (Issue eds.)
Buenos Aires, November 11-14, 2025

NUMERICAL INVESTIGATION OF THE ROLE OF PARTICLE SETTLING VELOCITY IN TURBIDITY CURRENTS

Santiago L. Zúñiga[a,b], M. I. Cantero[a,b,c] and S. Balachandar[d]

[a]*Instituto Balseiro, Universidad Nacional de Cuyo, San Carlos de Bariloche, Argentina.*

[b]*Comisión Nacional de Energía Atómica, San Carlos de Bariloche, Argentina.*

[c]*Consejo Nacional de Investigaciones Científicas y Técnicas, San Carlos de Bariloche, Argentina.*

[d]*Department of Mechanical and Aerospace Engineering, University of Florida, Gainesville, USA.*

Keywords: turbidity currents, sediment flow, dns, cfd, turbulence

Abstract. Turbidity currents are sediment-laden gravity flows that travel along the seafloor, driven by the excess density of suspended particles. They play a central role in shaping submarine landscapes and transporting sediment into the deep ocean, with significant implications for geology, ecology, and offshore oil prospecting. The dynamics of these flows depend critically on the interaction between turbulence, sediment suspension, and particle settling. This study investigates the role of particle settling velocity in modulating the structure and evolution of turbidity currents using direct numerical simulations (DNS) with approximately 100 million grid points and large eddy simulations (LES) of spatially evolving currents in extended domains (up to 1500 times the inlet height), solved via the spectral element method using the open-source solver Nek5000. We analyze a wide range of settling velocities on a shallow slope to isolate its impact on key flow properties such as velocity, concentration profiles, turbulent mixing, and entrainment. The results show that for sufficiently low values the flow behaves like a subcritical current. However, higher settling velocities lead to near-bed stratification and flow instabilities that manifest as internal hydraulic jumps with cyclic transitions between subcritical and supercritical regimes. For sufficiently high settling velocities, the flow permanently transitions to a supercritical state marked by persistent interfacial turbulence. The findings highlight the importance of settling velocity not only in controlling sediment deposition but also in governing the internal turbulence structure and entrainment of turbidity currents.

ISSN: 2591-3522 DOI: 10.70567/mc.v42.ocsid8497

1 INTRODUCTION

Turbidity currents are sediment-laden flows within submarine channels on gently sloping bottoms. The suspended sediments enhance density relative to clear fluid, increasing hydrostatic pressure and driving the flow downslope. The excess weight per unit volume drives the flow in the streamwise direction, while its bed-normal component stabilizes stratification. Mean shear generates turbulence, while stratification damps it.

For slopes $\theta \gtrsim 1^\circ$, conservative gravity currents approach a self-similar supercritical state with a near-wall turbulent layer and a turbulent interface layer. For $\theta \lesssim 1^\circ$, they evolve into a subcritical state, with layers separated by a thin destruction layer, only the near-wall layer being turbulent.

Turbidity currents differ due to sediment settling. The still-fluid settling velocity V_s plays a key role, though hindered settling is only important near the bed. Since the particle Stokes number $St \ll 1$, sediments effectively settle at V_s. Though small relative to turbulence, settling accumulates effects over long distances.

Settling introduces a downward sediment flux balanced by upward turbulent flux, producing a decreasing vertical concentration profile. Near the bed, the competition between sedimentation and resuspension dictates whether the current is depositional, erosional, or bypassing.

Recent studies have explored conservative currents across subcritical, supercritical, and transcritical regimes (Salinas et al., 2021b,a, 2020), but without settling. The purpose of this paper is to examine the role of settling velocity.

A non-zero V_s affects the current in two ways. First, unlike conservative currents where buoyancy flux is conserved, turbidity currents lose buoyancy downstream. Weak settling allows quasi-steady self-similar evolution, while strong settling can lead to momentum-dominated wall-jet-like flow (Necker et al., 2002; Nasr-Azadani and Meiburg, 2014). Second, settling alters vertical concentration, modifying driving force and stratification.

With a non-zero sediment settling velocity, the specification of the bottom sediment concentration boundary condition becomes important. Here we consider two limiting boundary conditions. In the first, the current is taken to be in the bypass mode with the resuspension flux precisely balancing the deposition flux at the bottom boundary. In this case, the streamwise sediment flux remains a constant within the current. In the second, the current is assumed to be fully depositional, with the resuspension flux being set to zero. The role of sediment settling velocity and the nature of the bottom boundary condition on the evolution of the current is examined in this study. Interesting evolutions, such as oscillatory onset of instability and transition from subcritical to supercritical state over the same slope, are observed.

2 SIMULATION DETAILS

We assume the density variation within the current to be sufficiently small that the use of the Boussinesq approximation is valid. Under this assumption, the governing equations take the form

$$\frac{\partial \mathbf{u}}{\partial t} + \mathbf{u}\cdot\nabla\mathbf{u} = -\nabla p + \frac{1}{Re_\tau}\nabla^2\mathbf{u} + \mathbf{g}c, \tag{1}$$

$$\nabla\cdot\mathbf{u} = 0\,, \tag{2}$$

$$\frac{\partial c}{\partial t} + (\mathbf{u}+\mathbf{V}_S)\cdot\nabla c = \frac{1}{\mathrm{Re}_\tau \mathrm{Sc}}\nabla^2 c. \tag{3}$$

These nondimensional equations are obtained using the inlet half-height H of the current as the length scale and the volume-averaged concentration c_v as the concentration scale, with

c denoting the local sediment concentration. The velocity scale is the shear velocity $u_\tau = \sqrt{g'H\sin\theta}$ (Cantero et al., 2009), where $g' = Rc_v g$ is the reduced gravity, g is the gravitational acceleration, and $R = \rho_s/\rho_f - 1$ is the relative density difference between sediment and fluid. The dimensionless parameters are $\mathrm{Re}_\tau = \dfrac{u_\tau H}{\nu}$, $\mathrm{Sc} = \dfrac{\nu}{\kappa}$, $\mathbf{g} = \{1, 0, -1/\tan\theta\}$ and $\mathrm{Ri}_\tau = \dfrac{g'\cos\theta H}{u_\tau^2}$. V_s is the nondimensional settling velocity of the sediment.

We report the results of DNS and LES numerical simulations of dilute turbidity currents flowing down a sloping bed of constant inclination, $\theta = 0.29°$, and $\mathrm{Ri}_\tau = 200$, $\mathrm{Re}_\tau = 180$ at the inlet. All simulations done using the spectral element method with the open source code Nek5000[1]. The boundary conditions used for the sediment at the bed are defined as:

Z BC:

$$\left.\frac{\partial c}{\partial z}\right|_{z=0} = 0. \tag{4}$$

We'll call this boundary condition *fully depositional* or zero-flux BC.

F BC:

$$\frac{1}{\mathrm{Re}_\tau \mathrm{Sc}} \left.\frac{\partial c}{\partial z}\right|_{z=0} = -\left|V_s c\right|_{z=0}\!\left|\,.\right. \tag{5}$$

This boundary condition is the same used by Cantero et al. (2009), also called *bypass mode* or *no net-deposition*.

A summary of the simulations performed can be seen in Table 1.

Case	V_s	Domain size	Number of elements	Type
V1F	1×10^{-3}	$300\times8.3\times10$	$336\times16\times34$	DNS
V2F	2×10^{-3}	$900\times8.3\times20$	$504\times8\times30$	LES
V3F	3×10^{-3}	$1500\times8.3\times25$	$840\times8\times30$	LES
V1Z	1×10^{-3}	$300\times8.3\times15$	$168\times8\times27$	LES
V2Z	2×10^{-3}	$300\times8.3\times15$	$168\times8\times27$	LES
V3Z	3×10^{-3}	$300\times8.3\times15$	$168\times8\times27$	LES
V20Z	2×10^{-2}	$1500\times8.3\times20$	$840\times8\times30$	LES
V50Z	5×10^{-2}	$1500\times8.3\times28$	$840\times8\times36$	LES
R200V0	0	$300\times8.3\times15$	$336\times16\times30$	DNS

Table 1: Cases studied in this work. Naming convention: VXB, where X is the settling velocity times 1×10^{-3} and C is the bottom BC. All cases computed with polynomial order $N = 8$.

3 RESULTS

3.1 Near self-similar profiles

On this section we will focus on the fully depositional **Z** boundary condition. We first define the streamwise fluxes of mass, momentum and buoyancy:

$$Q(x) = \int_0^\infty \overline{u}\,dz\,, \quad M(x) = \int_0^\infty \overline{u}^2\,dz\,, \quad F(x) = \int_0^\infty R\overline{cu}g\sin\theta\,dz\,. \tag{6}$$

[1]https://github.com/Nek5000/Nek5000

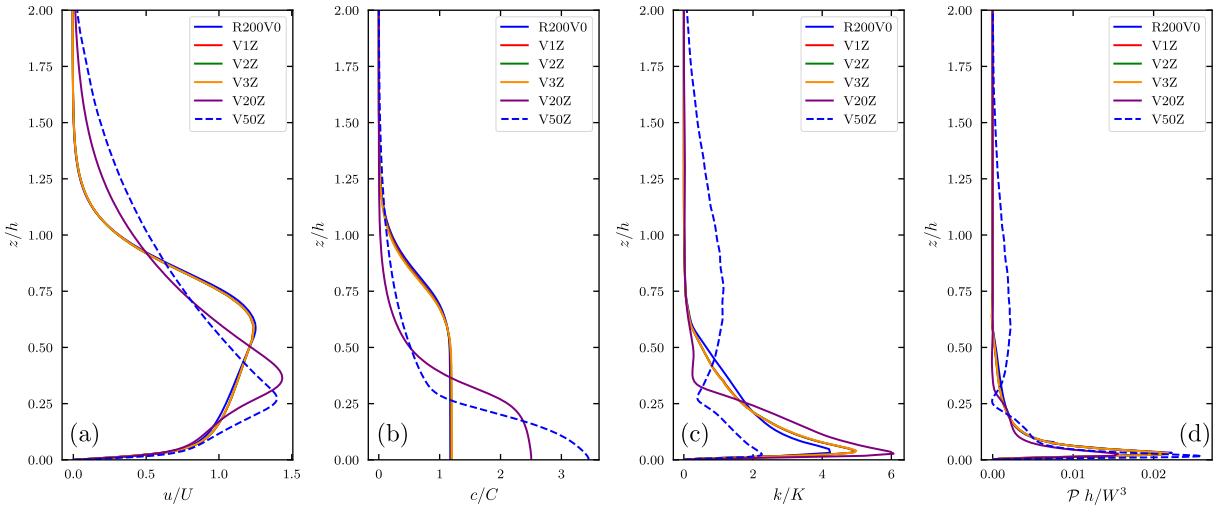

Figure 1: a) Mean streamwise velocity profiles scaled with depth-averaged streamwise velocity; b) mean concentration profiles scaled with depth-averaged concentration; c) mean turbulent kinetic energy profiles scaled with depth-averaged turbulent kinetic energy and d) mean turbulent kinetic energy production profiles scaled with depth-averaged production, as a function of z/h in the near self-similar state.

In the simulations, the upper limit is replaced with a large value of z that extends far upwards into the ambient, where the current velocity and buoyancy vanish. The fluxes are used to define current height $h(x) = Q^2/M$ and mean velocity $U(x) = M/Q$. We also define the mean kinetic energy flux $K = \int_0^\infty u\,k\,dz/Q$.

Figure 1a illustrates the near-self-similar profiles of scaled streamwise velocity as a function of z/h. For cases where $V_s < 3\times10^{-3}$, the settling effect is observed to be negligible. However, cases V20Z and V50Z exhibit a pronounced peak closer to the bed, followed by a more gradual decline towards the ambient fluid compared to the previous cases.

Figure 1b presents the self-similar profiles of scaled concentration as a function of z/h. When $V_s \leq 3 \times 10^{-3}$, the profiles are largely unaffected by settling, demonstrating strong agreement with those corresponding to a zero settling velocity. In contrast, the profiles for cases V20Z and V50Z display characteristics akin to those of a supercritical flow, wherein stratification effects are pronounced. Under these conditions, turbulence is maintained solely due to the imposed boundary conditions. As the turbidity current propagates downstream, it experiences continuous sediment loss, leading to progressive dilution.

Figure 1c depicts the self-similar profiles of turbulent kinetic energy (TKE) as a function of z/h. For cases with $V_s \leq 3 \times 10^{-3}$, the TKE profiles remain consistent, characterized by a near-wall peak and negligible values in the interface layer. Conversely, case V50Z demonstrates features resembling a supercritical flow, with a turbulent interface situated above the velocity maximum, facilitating active mixing of the ambient fluid into the current. Case V20Z is excluded from this plot as it does not exhibit a near-self-similar regime for TKE.

Finally, Figure 1d illustrates the self-similar profiles of scaled TKE production as a function of z/h. For cases where $V_s \leq 3 \times 10^{-3}$, the TKE production profiles show minimal variation. However, in case V50Z, the reduction in sediment concentration leads to decreased stratification, resulting in production profiles that resemble those of a supercritical current. In this scenario, turbulence is actively generated in the current interface (Salinas et al., 2021b).

3.2 Streamwise evolution

While all **Z BC** cases with $V_s \leq 3\times10^{-3}$ reach the near self-similar regime in the way expected from zero-settling simulations (Salinas et al., 2021a,b, 2022), cases V20Z and V80Z present a transitional behaviour akin to a transcritical case (Salinas et al., 2020). Figures 2a-e show the spanwise mean of instantaneous concentration for cases V0, V3Z, V20Z, V50Z and V80Z respectably. Also shown is the region with negative TKE production, representative of the thickness of the turbulence destruction layer (Salinas et al., 2021b), which diminishes in thickness at the regions with instabilities and, in the case V50Z, becomes very thin after the last instability, resembling a supercritical case. In the V20Z case we see repeated cycles where the overall height of the current slowly diminishes (i.e, $x = 200$ to 400, 500 to 900, 1000 and forward) followed by a sudden increase in interfacial mixing and turbulence, akin to an internal hydraulic jump, at $x \simeq 180$, 450, 950. In these regions, we see a sudden decrease in the thickness of the destruction layer, allowing turbulence to communicate between the bottom near-wall layer and the current interface. For case V50Z the behavior is similar, but after a last transition around $x = 400$ the current does not return to its previous subcritical regime, and remains with a growing active interface and a thin destruction layer.

3.3 Depth-averaged momentum balance

Following Parker et al. (1986); Shringarpure et al. (2012); Naqavi et al. (2018) we first investigate the dimensionless span and depth-averaged mean streamwise momentum equation. In the present case of steady flow regime, the mean streamwise momentum balance can be rigorously expressed in the following form without any approximation:

$$\frac{FQ}{\theta_m M} - \frac{C_D M^2}{Q^2} - \frac{d(\beta_p M)}{dx} - \frac{d(\beta_f M)}{dx} - e_w \frac{M^2}{Q^2} - Q\frac{dU}{dx} = 0 \tag{7}$$

In the above momentum balance, $C_D(x)$ is the basal drag coefficient, $e_w(x)$ is the entrainment coefficient, and $\theta_m(x)$, $\beta_p(x)$, and $\beta_f(x)$ are $O(1)$ shape factors, whose definitions and values in the self-similar regime are given in Salinas et al. (2022).

Figure 3 show the depth averaged momentum balance as a function of downstream location x for cases V20Z and V50Z. Case V20Z behaves very similarly to the transcritical case described in Salinas et al. (2020). Case V50Z, 3b, shows that after an initial set of oscillations, the flow goes on decelerating without reaching any sort of zero acceleration point in the domain. We also see that the main momentum source, $FQ/\theta_m M$ is constantly diminishing due to sediment leaving the domain at the bottom boundary condition. With this trend, i.e., diminishing momentum source due to sediment excess weight, increasing deceleration and increasing basal drag, it's expected that the current will reach a point where it will eventually die out.

3.4 Depth-averaged TKE balance

The dimensionless mean TKE balance in the statistically stationary state can be expressed as

$$\underbrace{\int_0^\infty \overline{P}\, dz}_{\delta_{f2}(M^3/Q^3)} - \underbrace{\int_0^\infty \overline{\varepsilon}\, dz}_{\psi_d(M^3/Q^3)} - \underbrace{\mathrm{Ri}_\tau \int_0^\infty \overline{w'c'}\, dz}_{\psi_f(M^3/Q^3)} - \underbrace{\frac{\partial}{\partial x}\int_0^\infty \overline{u}\overline{k}\, dz}_{dKQ/dx} \approx 0\,. \tag{8}$$

The first two terms are the TKE production and dissipation, where $\overline{P} = -\overline{u'_i u'_j}\frac{\partial \overline{u}_i}{\partial x_j}$ and $\overline{\varepsilon} = \frac{1}{\mathrm{Re}_\tau}\overline{\frac{\partial u'_i}{\partial x_j}\frac{\partial u'_i}{\partial x_j}}$, where overbar indicates span and time average and prime indicates fluctuation

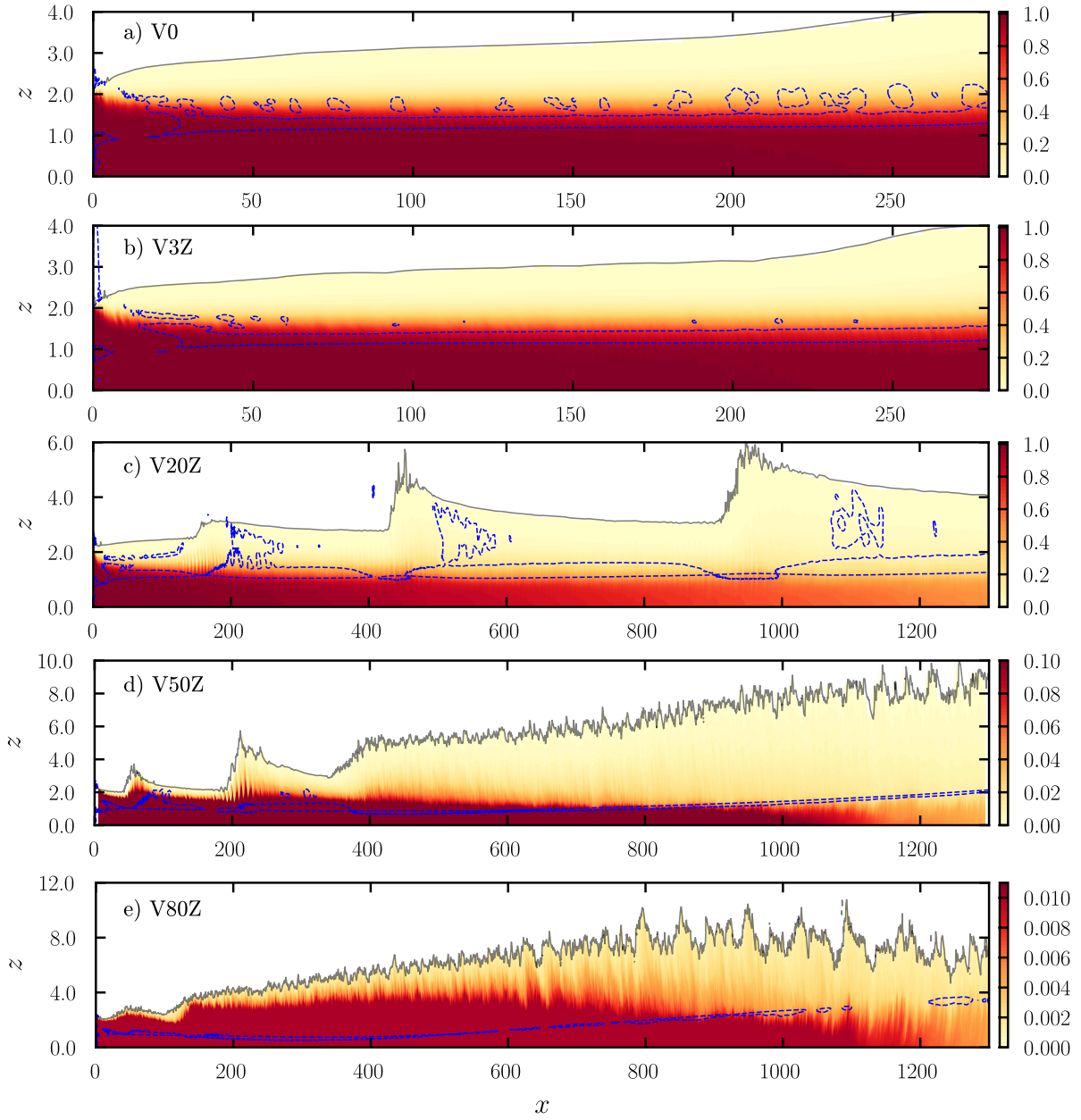

Figure 2: Spanwise averaged instantaneous concentration for cases V0, V3Z, V20Z, V50Z and V80Z. Wall-normal axis has been greatly stretched, and note the change in color scales between plots. The thin black line represents $c = 1\times10^{-3}$, and the blue lines where TKE production is zero.

about this mean. The other two terms are the wall-normal Reynolds flux and streamwise convection of TKE.

Figure 4 show the depth averaged TKE balance as a function of downstream location x for cases V3F, V20Z and V50Z. Dashed lines show the depth-average terms integrated up until the velocity maximum. Case V3F, 4a, shows a typical subcritical behavior except around $x = 875$ and $x = 1375$ where a small amount of turbulence production and, lagged behind it, TKE dissipation in the interface layer. This is related to a local decrease in thickness of the destruction layer, allowing the turbulence to communicate between the bottom bed layer and top interfacial layer. Case V20Z, 4b shows a similar behavior, but now TKE production and dissipation de-

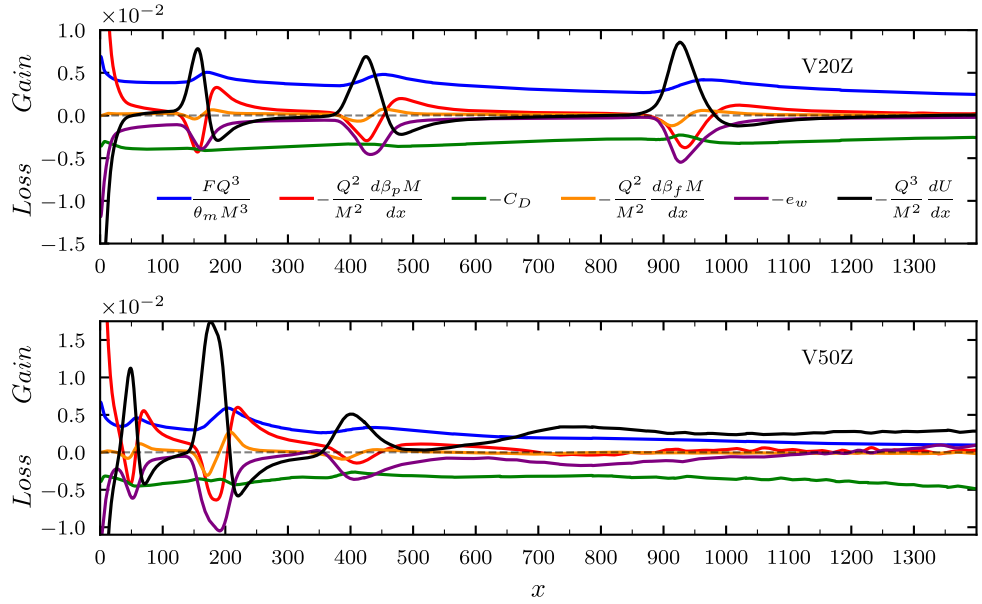

Figure 3: Depth averaged momentum balance as a function of downstream location x for cases with oscillations, V20Z and V50Z.

creases in magnitude in the downstream direction. The mechanics in each of the oscillations, around $x = 175$, $x = 425$ and $x = 950$ are the same that were observed in Zúñiga et al. (2022). Finally, case V50Z, 4c, shows that after the last oscillation, around $x = 750$, interfacial turbulence doesn't die out, and both production and dissipation are equally portioned between the near-wall layer and the interface layer. Interestingly, as we saw in 3b, this interfacial turbulence does not account for an increased ambient fluid entrainment e_w as one would expect. Another interesting characteristic of this case is a clear decrease in magnitude for turbulence statistics as we move downstream, supporting the claim that the current will eventually die out.

3.5 Depth-averaged sediment balance and partitioning

Dimensionless mean sediment balance in the statistically stationary state simplifies to

$$\underbrace{-\frac{\partial \overline{u}\,\overline{c}}{\partial x}}_{\text{Sm}} \underbrace{-\frac{\partial \overline{w}\,\overline{c}}{\partial z}}_{\text{Vm}} \underbrace{-\frac{\partial \overline{u'c'}}{\partial x}}_{\text{Sp}} \underbrace{-\frac{\partial \overline{w'c'}}{\partial z}}_{\text{Vp}} \underbrace{+V_s\frac{\partial \overline{c}}{\partial z}}_{\text{Se}} + \underbrace{\frac{1}{\text{ReSc}}\left(\frac{\partial^2 \overline{c}}{\partial x^2}+\frac{\partial^2 \overline{c}}{\partial z^2}\right)}_{\text{Di}} = 0. \tag{9}$$

From left to right the terms are sediment transport due to mean streamwise (Sm) and vertical (Vm) velocities, turbulent transport or Reynolds fluxes in the streamwise (Sp) and vertical (Vp) directions, transport due to particle settling (Se) and molecular diffusivity (Di). Depth-averaged sediment balance in the near bed layer is then given by four terms

$$-\frac{d}{dx}\int_0^{z_{max}} (\overline{uc}+\overline{u'c'})\,dz - (\overline{wc}|_{z_{max}} + \overline{w'c'}|_{z_{max}}) + V_s(\overline{c}|_{z_{max}} - \overline{c}|_0) + \frac{1}{\text{Re}_\tau \text{Sc}}\nabla^2\overline{c} \approx 0. \tag{10}$$

From left to right, each term accounts for sediment transport in the streamwise direction in the bottom layer; vertical sediment transport between the bottom and top layer; sediment stratification due to settling; and molecular diffusivity. Fig. 5 shows the previous balance as a function of downstream location x, scaled with $U\,C$, for cases V20Z and V50Z. We note that the other cases present a quick transition to a near self similar regime, where all terms become small.

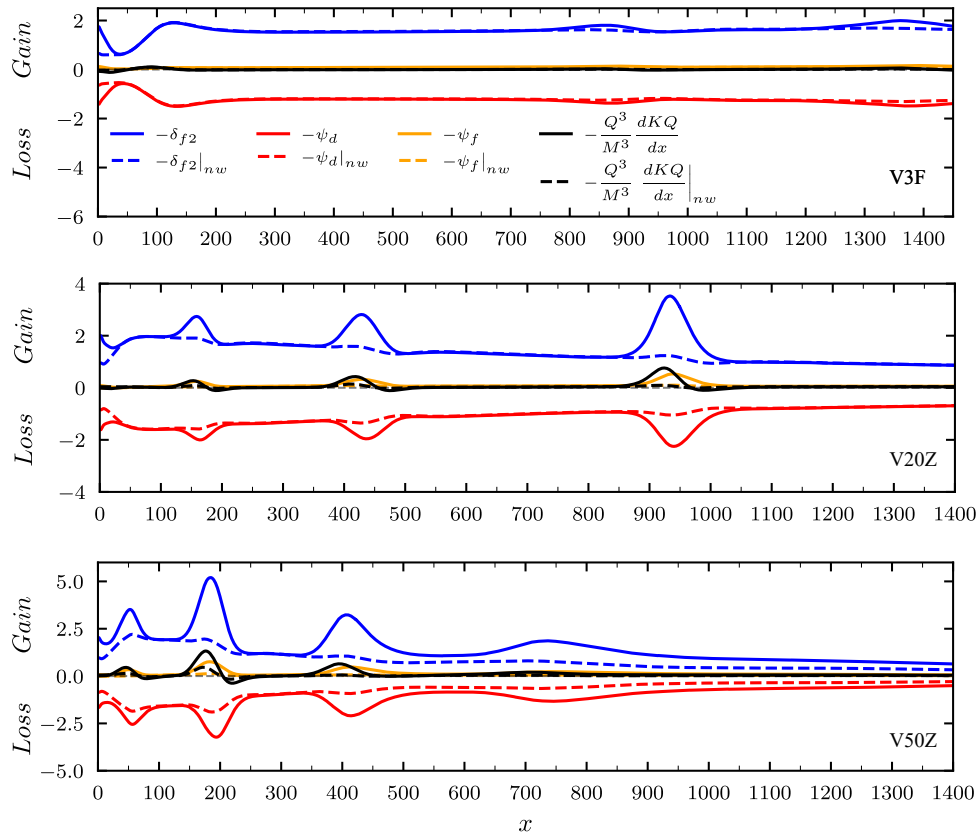

Figure 4: Depth averaged TKE balance as a function of downstream location x for cases with oscillations, V20Z and V50Z. Dashed lines show the depth-average terms integrated up until the velocity maximum.

After the oscillations, the vertical flux of sediment through the interface becomes negligible, and streamwise transport of sediment is almost completely balanced by settling of sediment due to V_s. In Fig. 6 the sediment balance resolved in the wall normal direction is shown, for the V20Z case at $x = 425$, 475 and 600, during different stages of the flow instability. We see the following behavior:

A. In the near-bed region, transport terms due to mean velocities are balanced. Just below the velocity maximum, there is a gain peak in turbulent vertical transport, which is balanced by molecular diffusivity. Particle settling is more important near the velocity maximum, where it's balanced almost entirely by a gain in mean vertical transport. The vertical turbulent transport term changes sign exactly at the velocity maximum, pushing sediment downwards below it and upwards above it.

B. Immediately after the previous region, the opposite occurs. We note that in this case the magnitude of all the transport terms is less than before, and turbulent transport plays a less important role. Some sediment is returned to the bottom layer, but less than it was originally sent upwards. Because of particle settling around the velocity maximum, the mean streamwise transport term reaches higher values.

C. Particle settling is the main source of sediment transport, moving particles downwards and all sediment balance terms slowly decline in magnitude, until the situation (A) occurs again.

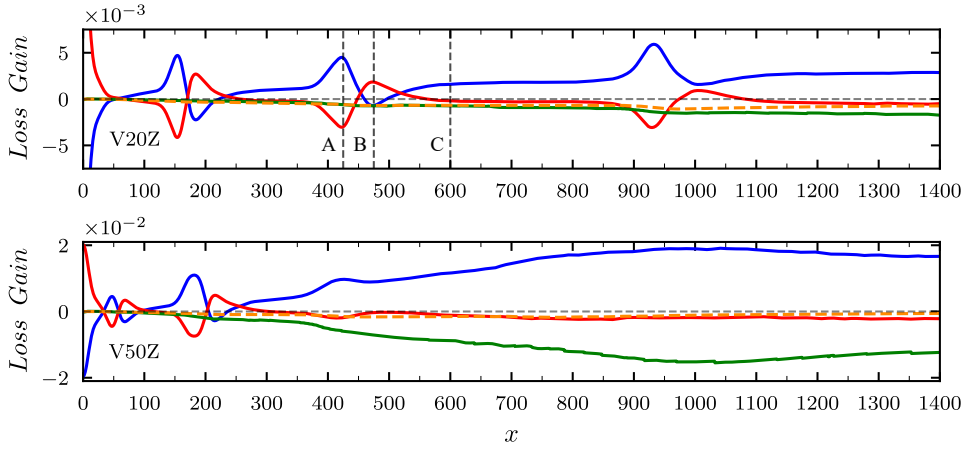

Figure 5: Scaled depth averaged sediment balance as a function of downstream location x for cases with oscillations, V20Z and V50Z, in the near wall layer. (—), $-\frac{d}{dx}\int_0^{z_{\max}} \overline{u}\,\overline{c}\,dz - \frac{d}{dx}\int_0^{z_{\max}} \overline{u'c'}\,dz$; (—), $-\overline{w}\,\overline{c}\big|_{z_{\max}} - \overline{w'c'}\big|_{z_{\max}}$; (—), $V_s\,\overline{c}\big|_{z_{\max}} - V_s\,\overline{c}\big|_{z=0}$; (– –), $\frac{1}{Re_\tau Sc}\nabla^2\overline{c}$. All terms are scaled with $U\,C$.

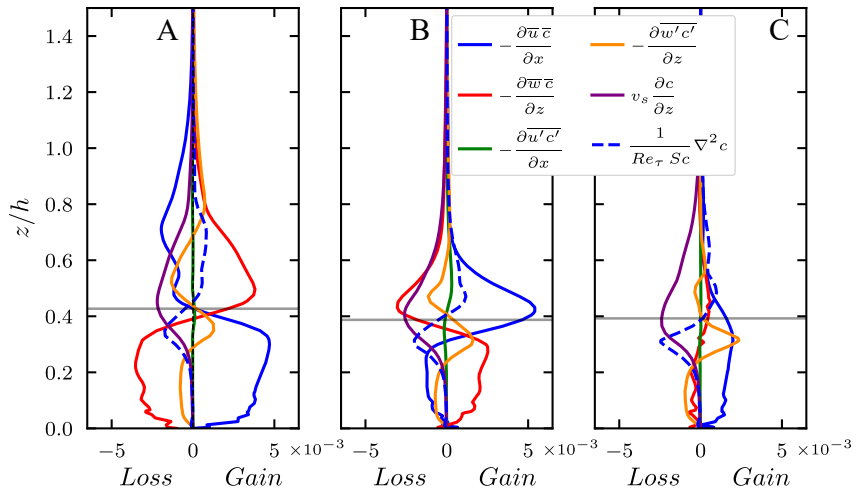

Figure 6: Sediment balance as a function of z/h for different locations near an instability for the V20Z case. The locations of the profiles are shown in the previous figure.

4 CONCLUSIONS

- From the near self-similar profiles for the fully depositional cases, settling effects are negligible for $V_s \leq 3 \times 10^{-3}$, resulting in velocity and concentration profiles consistent with zero-settling conditions. However, higher settling velocities ($V_s \geq 20 \times 10^{-3}$) introduce pronounced stratification and turbulence modifications, resembling supercritical flow dynamics.

- For intermediate cases (e.g., V20Z), instabilities manifest as internal hydraulic jumps with cyclic transitions between subcritical and supercritical regimes. In high settling cases like V50Z, the flow transitions permanently to a supercritical state downstream, characterized by a thin destruction layer and persistent interfacial turbulence.

- For low settling velocities, the momentum balance and TKE production align with zero-settling subcritical flows. Cases with oscillations (V20Z, V50Z) show decreasing mo-

mentum flux downstream, suggesting a gradual decay of the current, particularly for high settling velocities.

- High settling velocities lead to enhanced sediment deposition and reduced stratification downstream, progressively weakening the current. Sediment flux analysis confirms the diminishing role of turbulence and settling-induced stratification in high V_s cases, with the current eventually dying.

REFERENCES

Cantero M.I., Balachandar S., Cantelli A., Pirmez C., and Parker G. Turbidity current with a roof: Direct numerical simulation of self-stratified turbulent channel flow driven by suspended sediment. *Journal of Geophysical Research*, 114(C3), 2009. ISSN 0148-0227. http://doi.org/10.1029/2008JC004978.

Naqavi I.Z., Tyacke J.C., and Tucker P.G. Direct numerical simulation of a wall jet: flow physics. *Journal of Fluid Mechanics*, 852:507–542, 2018. http://doi.org/10.1017/jfm.2018.503.

Nasr-Azadani M.M. and Meiburg E. Turbidity currents interacting with three-dimensional seafloor topography. *Journal of Fluid Mechanics*, 745:409–443, 2014. ISSN 0022-1120, 1469-7645. http://doi.org/10.1017/jfm.2014.47.

Necker F., Härtel C., Kleiser L., and Meiburg E. High-resolution simulations of particle-driven gravity currents. *International Journal of Multiphase Flow*, 28(2):279–300, 2002. ISSN 03019322. http://doi.org/10.1016/S0301-9322(01)00065-9.

Parker G., Fukushima Y., and Pantin H.M. Self-accelerating turbidity currents. *Journal of Fluid Mechanics*, 171:145–181, 1986. http://doi.org/10.1017/S0022112086001404.

Salinas J., Balachandar S., Shringarpure M., Fedele J., Hoyal D., and Cantero M. Soft transition between subcritical and supercritical currents through intermittent cascading interfacial instabilities. *Proceedings of the National Academy of Sciences*, 117(31):18278–18284, 2020. ISSN 0027-8424, 1091-6490. http://doi.org/10.1073/pnas.2008959117.

Salinas J.S., Balachandar S., and Cantero M.I. Control of turbulent transport in supercritical currents by three families of hairpin vortices. *Physical Review Fluids*, 6(6):063801, 2021a. ISSN 2469-990X. http://doi.org/10.1103/PhysRevFluids.6.063801.

Salinas J.S., Balachandar S., Shringarpure M., Fedele J., Hoyal D., Zúñiga S., and Cantero M.I. Anatomy of subcritical submarine flows with a lutocline and an intermediate destruction layer. *Nature Communications*, 12(1):1649, 2021b. ISSN 2041-1723. http://doi.org/10.1038/s41467-021-21966-y.

Salinas J.S., Zúñiga S., Cantero M., Shringarpure M., Fedele J., Hoyal D., and Balachandar S. Slope dependence of self-similar structure and entrainment in gravity currents. *Journal of Fluid Mechanics*, 934:R4, 2022. http://doi.org/10.1017/jfm.2022.1.

Shringarpure M., Cantero M.I., and Balachandar S. Dynamics of complete turbulence suppression in turbidity currents driven by monodisperse suspensions of sediment. *Journal of Fluid Mechanics*, 427:1–34, 2012. http://doi.org/10.1017/jfm.2012.427.

Zúñiga S.L., Salinas J.S., Balachandar S., and Cantero M.I. Universal nature of rapid evolution of conservative gravity and turbidity currents perturbed from their self-similar state. *Physical Review Fluids*, 7(4):043801, 2022. ISSN 2469-990X. http://doi.org/10.1103/PhysRevFluids.7.043801.